Wave space resolution in ultrasonic scattering measurements

T. Douglas Mast
Department of Electrical Engineering, University of Rochester, Rochester, New York 14627

Robert C. Waag
Departments of Electrical Engineering and Radiology, University of Rochester, Rochester, New York 14627

(Received 12 September 1994; accepted for publication 22 June 1995)

The spatial-frequency spectra of the spatial properties of a scattering medium can be determined from measurements of scattering over a number of angles or frequencies. In such measurements, the spatial localization associated with transducer beam patterns and time gates causes an uncertainty in the measured spatial-frequency domain properties of the scatterer. This uncertainty is analyzed using an analytic and computational model in which system effects are represented by a spatial-frequency domain function. Wave space resolution in a particular direction is shown to be inversely proportional to the spatial-frequency spread of the system function in that direction. In the backscatter case, wave space resolution is limited in the direction of the scattering vector by a convolution of the emitted pulse and the detector time gate, and resolution in the lateral direction depends mainly on the transducer aperture, increasing approximately in proportion to the aperture diameter. In the case of backscatter measurements, smooth aperture apodization improves lateral resolution somewhat but has little effect on resolution in the direction of the scattering vector. For angular scattering measurements, resolution in all directions depends on both the aperture size and (for sufficiently short time gates) on the time gates employed. Illustration of the practical importance of wave space resolution is provided using analysis of two previously published tissue characterization experiments.

PACS numbers: 43.80.Ev, 43.80.Vj

INTRODUCTION

The acoustic scattering caused by a given inhomogeneous object may, under the proper circumstances, be correlated directly with the spatial-frequency spectrum of the object's inhomogeneities. More specifically, for weakly scattering media, the scattered field corresponds to a spatial Fourier transform of the medium variations. Since the early 20th century, measurements of x-ray diffraction based on this principle have been used for materials characterization.[1]

The potential of ultrasonic scattering measurements for tissue characterization has been recognized since the 1970s.[2–6] Since that time, the theoretical basis for the determination of tissue structure from scattering measurements has been laid by a number of investigators considering backscatter[7–15] and angular scattering[16–20] configurations. Because disease can affect the acoustic scattering properties of certain tissues, tissue characterization of this kind has potential use as a diagnostic tool. Experimental techniques based on this principle have been implemented for diagnosis of disease in cardiac tissue,[21–23] liver,[22,24–26] kidney,[25] breast tissue,[27] and skeletal muscle.[28]

The principle behind tissue characterization from ultrasonic scattering is that scattering measurements can be used to estimate the spatial-frequency properties of tissue. For weak scattering, the average differential scattering cross section for a given angle and frequency is approximately proportional to the spatial-frequency spectrum of the medium variations for a given value of the scattering vector,[29] which is defined to be the difference of the incident wave vector and the scattered wave vector. In the case of backscatter measurements, the temporal-frequency dependence of the backscatter coefficient is approximately proportional to the spatial-frequency dependence of the spectrum of the medium variations.

These relations are approximate, even for weak scattering, since in practical scattering measurement systems the incident wave is a beam rather than a plane wave, the scattered field is detected over a finite aperture rather than at a point, the incident wave has a finite duration, and detection occurs over a finite temporal interval. These deviations from the ideal situation have the result that the measured scattered field is not directly proportional to the spatial-frequency spectrum of the scatterer properties. Instead, the measured field can be interpreted as an integral of this spectrum weighted by a function that represents the measurement system effects.

The effect of the measurement system is usually assumed to be equivalent to a frequency- and angle-dependent scaling of the scattering data. The theories cited above[7–19] include methods to remove this scaling so that intrinsic scatterer properties such as the differential scattering cross section or backscatter coefficient can be determined from scattering measurements. Such an approach requires the implicit assumption that removal of measurement system dependences yields an accurate approximation of the scatterer properties. Scattering measurements for which this assumption is invalid cannot be normalized to accurately obtain intrinsic scatterer properties, so that such measurements may not be useful for tissue characterization.

The validity of this assumption is examined in the present paper using a previously developed model[18,19] for

system effects in ultrasonic scattering measurements. In this model, the system effects are represented in the spatial-frequency and temporal-frequency domains by a ''system function.'' Because the acoustic fields do not cover all of real space, the system function is not concentrated at a point in wave space, but has a finite spread. This wave space spread causes a loss of resolution in measurements of the spatial-frequency properties of a scatterer. When resolution is lost, features in the spatial-frequency spectrum of the scattering object are blurred and useful diagnostic information may be lost. When the system function spread is comparable to the spread of the spatial-frequency properties of the scattering object, accurate measurement of the spatial-frequency properties of the object is impossible. For these reasons, consideration of wave space resolution is important for the design of quantitative imaging and tissue characterization measurements.

Section I of this paper briefly reviews the theory presented in Refs. 18 and 19 and develops a link between system function properties and wave space resolution. Detailed system function computations are outlined in Sec. II and computational results are presented in Sec. III. The effect of wave space resolution limitations on tissue characterization and quantitative imaging experiments is discussed in Sec. IV in the context of two previously published experiments.

I. THEORY

Below, the usual ideal, approximate relations used in tissue characterization measurements are briefly stated. More general expressions[18,19] for the relations between measured scattering and spatial-frequency spectra of tissue are then summarized. These general expressions are then used to derive the relationship between the achievable spatial-frequency resolution and the properties of the measurement system used in a scattering experiment.

The present theory treats measurement of scattering from inhomogeneous media. The inhomogeneities considered consist of local variations in compressibility κ and in density ρ, defined, respectively, as

$$\gamma_\kappa = \frac{\kappa - \kappa_0}{\kappa_0}, \quad \gamma_\rho = \frac{\rho - \rho_0}{\rho}, \tag{1}$$

where κ_0 is the ambient compressibility and ρ_0 is the ambient density.

For single-frequency, plane-wave incidence, point reception in the far field of the scattering region, and when $\gamma_\kappa \ll 1$ and $\gamma_\rho \ll 1$ (so that the Born approximation holds), the scattered pressure is[29]

$$p_s(\mathbf{K}_0) = A 2\pi^2 k_0^2 (e^{ik_0 r}/r)\Gamma(-\mathbf{K}_0). \tag{2}$$

Here $k_0 = \omega_0/c$ is the wave number of the incident wave where ω_0 is the radial frequency and c is the speed of sound outside the inhomogeneous region. The amplitude of the incident wave is denoted by A. The distance r is the magnitude of a vector $\mathbf{r}$ pointing to the measurement point from the origin. The reference scattering vector $\mathbf{K}_0$ is defined as

$$\mathbf{K}_0 = \mathbf{I}_0 - \mathbf{O}_0, \tag{3}$$

where $\mathbf{I}_0$ is a vector of magnitude k pointing in the direction of propagation of the incident wave and $\mathbf{O}_0$ is a vector of magnitude k and the same direction as $\mathbf{r}$. The reference scattering vector has the magnitude

$$K_0 = 2(\omega_0/c)\cos(\theta), \tag{4}$$

where 2θ is the angle between the emitter and the detector, as sketched later in Fig. 2. The function $\Gamma(\mathbf{K}_0)$ is the three-dimensional Fourier transform of the variation function

$$\gamma(\mathbf{r}) = \gamma_k(\mathbf{r}) + \frac{\mathbf{I}_0 \cdot \mathbf{O}_0}{k_0^2}\,\gamma_\rho(\mathbf{r}). \tag{5}$$

Equations (2)–(5) have the result that in backscatter measurements ($\theta = 0$), the frequency-dependent backscatter coefficient is directly proportional to the spectrum of the medium variations, while in angular scattering measurements this spectrum can be determined from the angular dependence of scattering.

For the case of statistically homogeneous or stationary random scattering media, the power spectrum of the medium variations may be defined as the Fourier transform of the autocorrelation function of the medium variations:

$$S_\gamma(\mathbf{K}_0) = \frac{1}{(2\pi)^3}\int_V \langle \gamma(\mathbf{r}')\gamma(\mathbf{r}'+\mathbf{r})\rangle e^{-i\mathbf{K}_0\cdot\mathbf{r}}\, d^3r. \tag{6}$$

When the ''ideal'' conditions listed before Eq. (2) are valid, the scattered power (averaged over many realizations of the scattering medium) is directly proportional to the spatial-frequency spectrum of the medium variations. This proportionality is governed by the relation[29]

$$\bar{\sigma}_d(\mathbf{K}_0) = (k_0^4 \pi/2) S_\gamma(\mathbf{K}_0), \tag{7}$$

where the average differential scattering cross section $\bar{\sigma}_d(\mathbf{K}_0)$ is defined as the average scattered power for unit intensity, solid angle, and scatterer volume.

The foregoing simple relationships no longer hold when the incident wave is not planar, when the area of detection is finite, or when the times of transmission and detection are finite. In this nonideal case, expressions analogous to Eqs. (2) and (7) are[18,19]

$$P_m(\mathbf{K}_0, \omega_0) = \int_{\mathbf{K}} \Gamma(-\mathbf{K}, \omega_0)\Lambda_W(\mathbf{K}, \mathbf{K}_0, \omega_0) d^3K \tag{8}$$

for the case of scattering media with well-defined Fourier transforms and

$$\langle |P_m(\mathbf{K}_0, \omega_0)|^2 \rangle = \int_{\mathbf{K}} S_\gamma(\mathbf{K}, \omega_0) |\Lambda_W(\mathbf{K}, \mathbf{K}_0, \omega_0)|^2\, d^3K \tag{9}$$

for the case of statistically homogeneous scattering media. The measured quantity is now taken to be $P_m(\mathbf{K}_0, \omega_0)$, the temporal harmonic spectrum of the measured pressure integrated over the surface of the receiving transducer. The variables of integration are the components of the scattering vector $\mathbf{K}$, defined as $\mathbf{I} - \mathbf{O}$ where the variable local vectors $\mathbf{K}$, $\mathbf{I}$, and $\mathbf{O}$ are defined in a manner analogous to the constant reference vectors $\mathbf{K}_0$, $\mathbf{I}_0$, and $\mathbf{O}_0$. Here the general wideband ''system function'' Λ_W, which incorporates the effects of fi-

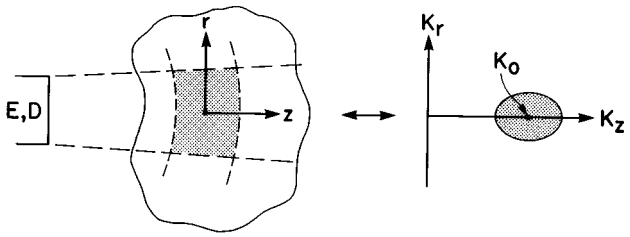

FIG. 1. Backscatter geometry. In the left panel, a transducer serving as emitter E and detector D probes a scattering object. The effective scattering region, defined by the transducer's beam pattern, pulse length, and receiver time gate, is denoted by stippling. In the right panel, the wave space representation of this scattering system is shown. The spread of the effective scattering region in real space corresponds in wave space to a concentration, denoted by stippling, around the scattering vector $\mathbf{K}_0$.

nite emitter and detector beam patterns and time gates, is given by

$$\Lambda_W(\mathbf{K},\mathbf{K}_0,\omega_0)=(2\pi)^4 k_0^2 \int W_E(\omega)W_D(\omega_0-\omega)\left[\frac{i\omega\rho}{4\pi} \times \int V_E(\boldsymbol{\nu})V_D(\boldsymbol{\eta})e^{iz_E\nu_3}e^{iz_D\eta_3}\, d\phi\right] d\omega, \tag{10}$$

where W_E and W_D are temporal spectra of the emitter waveform and the detector time gate, V_E and V_D are angular spectra of the emitter and detector velocity beam patterns, and z_E and z_D are distances from the origin to the emitter and detector. Definitions for the spatial-frequency vectors $\boldsymbol{\nu}$ and $\boldsymbol{\eta}$, their components ν_3 and η_3, and the angle ϕ as well as the limits of the ϕ integration are given in Ref. 18. The vectors $\boldsymbol{\nu}$ and $\boldsymbol{\eta}$ are functions of ϕ. The quantity within the square brackets is defined to be $\Lambda(\mathbf{K},\mathbf{K}_0,\omega_0)$ and is called the beam intersection function since it represents a wave space product of emitter and detector beam functions.

Sketches of the scattering geometry in real space and wave space are given in Figs. 1 and 2 for backscatter and angular scattering configurations, respectively. In the backscatter case, the extent of the scattering region in range is determined by the emitter and detector time gates and the extent in azimuth is determined by the emitter and detector beam patterns. In the angular scattering case shown, the scattering region is defined by the intersection of the emitter and detector beams. The effective scattering region may also, in general, be influenced by the emitted waveform and the detector gate. In any case, the finite extent of the scattering region in real space corresponds to a finite spread of the beam intersection function in wave space about the point corresponding to the reference scattering vector $\mathbf{K}_0$.

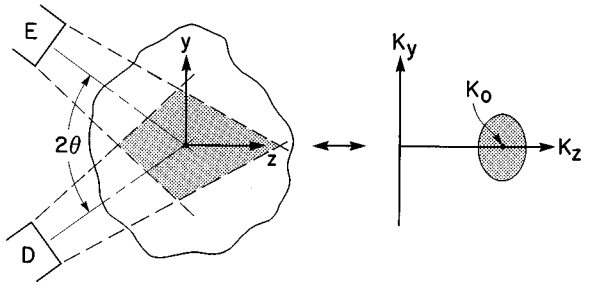

FIG. 2. Angular scattering geometry. In the left panel, an emitter E and a detector D, separated by an angle 2θ, probe a scattering object. The effective scattering region, denoted by stippling, is defined by the intersection of the emitter and detector beams. The right panel shows the wave space representation of this system, in which the real-space spread of the effective scattering region corresponds in wave space to a concentration, denoted by stippling, about the scattering vector $\mathbf{K}_0$.

In the derivation below, an arbitrary vector $\mathbf{K}$ is represented by its Cartesian components K_1, K_2, and K_3, or, equivalently, K_x, K_y, and K_z. The x direction is defined as perpendicular to the y and z directions, so that in Fig. 2 the K_x axis points into the page. The K_r component of a vector $\mathbf{K}$, as shown in Fig. 1, is defined as $\sqrt{K_1^2+K_2^2}$.

When all significant contributions to the ω integration come from the frequency region where $|\omega-\omega_0|/\omega_0 \ll 1$ and when the overall spread of Λ is small with respect to k, Λ_W can be approximately represented by the narrow-band system function[19]

$$\Lambda_N(\mathbf{K},\mathbf{K}_0,\omega_0) = (2\pi)^4 k_0^2 \int \Lambda\left[\left(\mathbf{K}-2\,\frac{\omega-\omega_0}{c}\cos\,\theta\mathbf{i}_3\right),\mathbf{K}_0,\omega_0\right] \times W_E(\omega)W_D(\omega_0-\omega)e^{i\omega(z_E+z_D)/c}\, d\omega. \tag{11}$$

Here, $\mathbf{i}_3$ is the unit vector in the K_3 direction. In this case, the narrow temporal-frequency spectra of the emitter and detector beams and the narrow spatial-frequency extent of Λ allow the K_3 integration to be represented by a convolution in the temporal frequency ω.

For the case of an infinite detector time gate, W_D takes the form of a Dirac delta function and the system function Λ_W simplifies to the form

$$\Lambda_A=(2\pi)^4 k_0^2 W_E(\omega_0)e^{ik_0(z_E+z_D)}\Lambda(\mathbf{K},\mathbf{K}_0,\omega_0). \tag{12}$$

Thus, in the case of an infinitely long detector gate, the spread of the system function depends only on the characteristics of the emitter and detector beams, while the finite duration of the emitter waveform affects the system function only through a multiplicative constant.

The spectral functions $\Gamma(\mathbf{K}_0)$ and $S_\gamma(\mathbf{K}_0)$ can be estimated from scattering measurements if Λ_W is concentrated near one point in wave space and if Γ and S_γ are slowly varying relative to Λ_W. Then the effect of Λ_W in the integrals of Eqs. (8) and (9) is like that of a Dirac delta function. In this case, the spectra may be estimated as

$$\Gamma(\mathbf{K}_0,\omega_0)\approx P_m(-\mathbf{K}_0,\omega_0)/\mathbf{H}^V_{(\cdot)} \tag{13}$$

and

$$S_\gamma(\mathbf{K}_0,\omega_0)\approx\langle|P_m(\mathbf{K}_0,\omega_0)|^2\rangle/|H_{(\cdot)}|^2, \tag{14}$$

respectively, where

$$H^V_{(\cdot)}=\int_{\mathbf{K}}\Lambda_{(\cdot)}\, d^3K, \tag{15}$$

$$|H_{(\cdot)}|^2=\int_{\mathbf{K}}|\Lambda_{(\cdot)}|^2\, d^3K, \tag{16}$$

and $(\cdot)$ represents W, A, or N.

In Eqs. (15) and (16), the overall system effects at one spatial-frequency point $\mathbf{K}_0$ are approximated by an integration of a system function $\Lambda_{(\cdot)}$ over all wave space. These approximations are strictly valid only in the limit where the system function $\Lambda_{(\cdot)}$ is tightly concentrated at one point in wave space. For realistic measurement systems, when Eq. (15) or (16) is used to estimate the spatial-frequency properties of a scattering object or region, error results from the finite extent of the functions $\Lambda_{(\cdot)}$ in wave space. This error has the effect of decreasing the spatial-frequency resolution that can be achieved. When the spatial-frequency resolution is inadequate, certain features of the spatial-frequency spectrum of the scatterer properties (for instance, peaks in the spectrum corresponding to nearly periodic spacings of correlated inhomogeneities) will not be resolved.

The specific link between system function spread and wave space resolution is shown in the following derivation. The general problem of resolving features of scattering object spatial-frequency spectra is represented in this derivation by a simple canonical problem. The spatial-frequency spectrum of the scattering object is taken to be a sum of Dirac delta functions, corresponding to two dominant spatial-frequency components in the spectrum. This can be regarded as a fundamental limiting case of the problem of resolving narrow features of the spatial-frequency spectrum.

Consider a Gaussian system function (written, for convenience, without constant coefficients) such that

$$|\Lambda_{(\cdot)}|^2 = e^{-|\mathbf{K}-\mathbf{K}_0|^2/(2\alpha^2)} \tag{17}$$

and a scattering region for which S_γ is comprised of two Dirac delta functions, which may be assumed without loss of generality to be located along the $\mathbf{i}_3$ axis, such that

$$S_\gamma(\mathbf{K}_0,\omega_0) = \delta[(K'-\epsilon)\mathbf{i}_3 - \mathbf{K}_0] + \delta[(K'+\epsilon)\mathbf{i}_3 - \mathbf{K}_0], \tag{18}$$

where ϵ is an arbitrary spatial-frequency parameter. The function S_γ may be estimated by measuring $\langle|P_m(\mathbf{K}_0)|^2\rangle$ for scattering vectors $\mathbf{K}_0$ having direction $\mathbf{i}_3$ (which corresponds to backscatter measurements) and varying magnitude K_0.

Then, from Eq. (9), the spectrum of the measured pressure is

$$\langle|P_m(K_0)|^2\rangle = 2e^{-(K_0^2 - 2K'K_0 + K'^2 + \epsilon^2)/(2\alpha^2)} \cosh\frac{\epsilon(K_0-K')}{\alpha^2}. \tag{19}$$

The measured spectrum $\langle|P_m|^2\rangle$ will resolve the two peaks only if α is sufficiently small. The absolute limit beyond which the peaks cannot be resolved is the value of α for which $d^2\langle|P_m|^2\rangle/dK_0^2$ is equal to zero; this occurs for $\alpha=\epsilon$, so that peaks separated by less than 2α cannot be resolved.

The increase of resolution with decreasing α can be quantified by examining the ratio of $\langle|P_m|^2\rangle$ evaluated at one of the peaks and $\langle|P_m|^2\rangle$ evaluated at the central point between the peaks:

$$\frac{\langle|P_m(K'+\epsilon)|^2\rangle}{\langle|P_m(K')|^2\rangle} = \frac{1}{2}\, e^{\epsilon^2/(2\alpha^2)}(1+e^{-2\epsilon^2/\alpha^2}). \tag{20}$$

This ratio takes a value of $\sqrt{2}$ (3 dB) for $\alpha=0.70\,\epsilon$ and takes a value of 2 (6 dB) for $\alpha=0.60\epsilon$, so that spatial-frequency features are resolvable by 3 dB if separated by more than 2.9 α and are resolvable by 6 dB if separated by more than 3.3 α.

In general, the spread of $|\Lambda_{(\cdot)}|^2$ in a given direction may be described by the second central moment in that direction, given by[18]

$$\sigma_n^2(|\Lambda_{(\cdot)}|^2) = \frac{\int_{\mathbf{K}}(K_n - \mathbf{i}_n\cdot\mathbf{K}_0)^2|\Lambda_{(\cdot)}(\mathbf{K})|^2\, d^3K}{\int_{\mathbf{K}}|\Lambda_{(\cdot)}|^2\, d^3K}, \tag{21}$$

where $n=1$, 2, or 3.

For the Gaussian form of $|\Lambda_{(\cdot)}|^2$ given in Eq. (17), the second central moment in each direction is simply α^2. In this case, for estimates of the spectrum S_γ, spectral features spaced more closely in the direction $\mathbf{i}_n$ than $2\sigma_n(|\Lambda_{(\cdot)}|^2)$ cannot be resolved. For other forms of $|\Lambda_{(\cdot)}|^2$, the second central moment provides an estimate of the system function spread that is analogous to the Gaussian parameter α as long as $|\Lambda_{(\cdot)}|^2$ is concentrated in the region of its main peak. This is the case for all the system functions to be examined in this paper so that, for all cases examined here, the second central moment in a given direction, as defined by Eq. (21), is used to obtain an estimate of the achievable wave space resolution.

Asymptotic results for Gaussian apertures and time gates have been previously described.[19] These results were derived for the case in which the emitter size is equal to the detector size and the Gaussian parameter of the emitted pulse is equal to that of the detector time gate. The asymptotic approximations made were consistent with the assumptions that the system function $\Lambda_{(\cdot)}$ is concentrated over a small region in wave space and that the emitter and detector time gates are sufficiently long for the narrow-band approximation to be applicable. These assumptions are validated by the good agreement of the asymptotic and exact results obtained for Gaussian apertures.

The asymptotic results given in Ref. 19 are briefly summarized here for convenient reference, using the symbols H and $\wedge$ to denote the asymptotic forms of H and Λ. However, the corresponding equations for H_N^V and H_A^V in Ref. 19 are in error by a factor of $(2\pi)^4$ while those for $|\mathsf{H}_N|^2$ and $|\mathsf{H}_A|^2$ are in error by factors of $(2\pi)^8$; these errors are corrected in the following equations.

The assumptions behind the following equations are that the system function Λ is concentrated near one point in wave space, so that a spatial-frequency analog of the Fresnel approximation may be used, and that the narrow-band approximation is valid. Under these conditions, for Gaussian apertures with Gaussian parameter α and time gates with Gaussian parameter α_t and nondimensional amplitude A_t,

$$\mathsf{H}_A^V(\mathbf{K}_0,\omega_0) = \frac{i2^2\pi^3\rho A_0\omega_0 W_E(\omega_0)e^{i2k_0z}}{(1+iz/k_0\alpha^2)^2}, \tag{22}$$

$$|\mathsf{H}_A(\mathbf{K}_0,\omega_0)|^2 = \frac{2^{1/2}\pi^{9/2}\rho^2A_0^2\alpha^3\omega_0^2|W_E(\omega_0)|^2}{[1+(z/k_0\alpha^2)^2]^{1/2}}\,\frac{1}{\sin 2\theta}, \tag{23}$$

$$\mathsf{H}_N^V(\mathbf{K}_0,\omega_c) = \frac{i2\pi^{5/2}\rho A_0A_t^2\alpha_t\omega_c e^{i2k_cz}}{(1+iz/k_c\alpha^2)^2}, \tag{24}$$

$$|H_N(\mathbf{K}_0,\omega_c)|^2=\frac{2^{-5/2}\pi^{7/2}\rho^2 cA_0^2A_t^4\alpha_t^3\alpha^2\omega_c^2}{\{[1+(z/k_c\alpha^2)^2][1+(c\alpha_t\tan\theta)^2/\alpha^2+(z/k_c\alpha^2)^2]\}^{1/2}}\frac{1}{\cos^2\theta}, \tag{25}$$

$$\sigma_1(|\wedge_{(\cdot)}|^2)=\frac{1}{\alpha},\quad \sigma_2(|\wedge_{(\cdot)}|^2)=\frac{\cos\theta}{\alpha}, \tag{26}$$

and

$$\sigma_3(|\wedge_{(\cdot)}|^2)=\sqrt{\frac{1}{(c\alpha_t)^2}\cos^2\theta+\frac{1}{\alpha^2}\sin^2\theta}. \tag{27}$$

As shown above, wave space resolution in the ith direction for a given measurement system is proportional to $1/\sigma_i$. Thus Eqs. (26) and (27) lead to the conclusion that the wave space resolution limit achievable with Gaussian transducers is approximately inversely proportional to the aperture size of the transducer except in the backscatter direction. There, the resolution limit in the lateral direction is approximately inversely proportional to the aperture size while the resolution limit in the axial direction is inversely proportional to the time gate length. For other transducers, analogous asymptotic results imply that the wave space resolution limit is approximately inversely proportional to the aperture size (although by a different constant) as long as the assumptions behind Eqs. (22)–(27) are valid. As seen from Eq. (27), however, short time gates will further decrease the wave space resolution achieved in angular scattering experiments.

II. COMPUTATIONAL METHOD

Computations of $\Lambda(\mathbf{K},\mathbf{K}_0,\omega_0)$ and $\Lambda_N(\mathbf{K},\mathbf{K}_0,\omega_0)$ were carried out for axially symmetric Gaussian, exponential, and uniform (disk) emitters and detectors in backscatter and angular scattering configurations.

The apertures were defined such that for equivalent radii r_{eq}, the total emitted power and the far-field on-axis amplitude were equal. Without loss of generality, the emitter velocity amplitude and detector sensitivity were taken to be unity for the disk apertures. For the equivalence conditions to hold, the apodizations $f(r)$ (emitter velocity distribution and detector sensitivity patterns) are as follows:

$$f(r)=\begin{cases} u(r_{\text{eq}}-r) & \text{(disk)},\\ 4e^{-r/a}, \quad a=r_{\text{eq}}/(2\sqrt{2}) & \text{(exponential)},\\ 2e^{-r^2/(2\alpha^2)}, \quad \alpha=r_{\text{eq}}/2 & \text{(Gaussian)}, \end{cases} \tag{28}$$

where u represents the Heaviside step function and r is the magnitude of a vector $\mathbf{r}$ directed from the origin to a point on the emitter or detector surface.

Constant parameters in the calculations were $f=5.0$ MHz, $z=135$ mm, $c=1.503$ mm/μs, and $\rho=0.001$ g/mm^3. The only parameters varied were the angle, transducer size, and time gate length, since these quantities control the spread of the system function and therefore the wave space resolution. Variations in frequency and distance affect the magnitudes of the normalization integrals but do not strongly affect the spread of the system function.[19]

Backscatter calculations were carried out for effective transducer radii of 3.175, 6.5, and 10 mm and for Gaussian time gate parameters of 3 and 6 μs as well as infinite time gates. In all cases, the emitter and detector time gate parameters were equal. Angular calculations were carried out using effective radii of 6.5 mm and angles of 33°, 48°, and 60°. These angles, together with the backscatter calculations, correspond to evenly spaced steps between 3.33 and 6.65 cy/mm in the spatial-frequency variable $K/2\pi$.

The narrow-band system function Λ_N was not calculated for the angular scattering configurations examined here because the spread of the system functions in these cases is primarily determined by the aperture characteristics, because

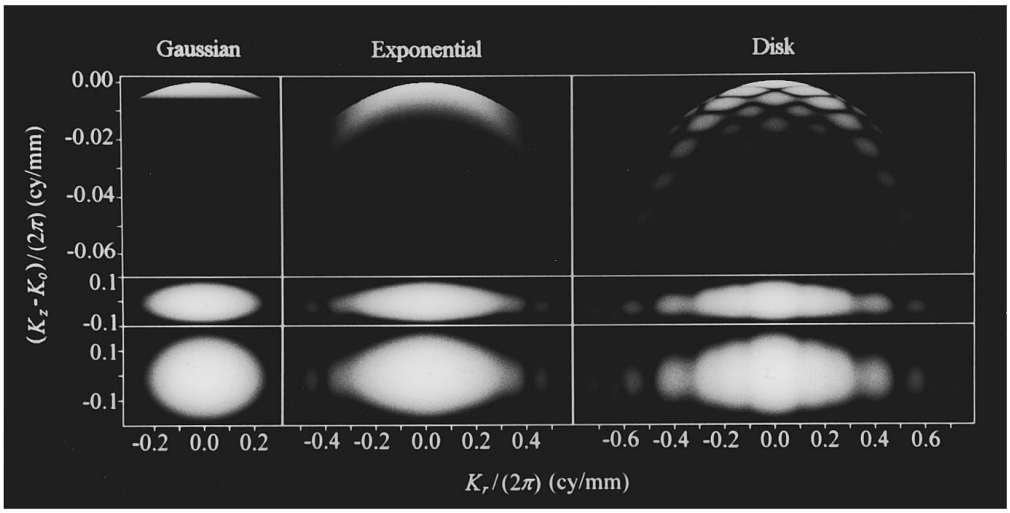

FIG. 3. System function magnitudes for 6.5-mm Gaussian, exponential, and disk apertures in backscatter configuration. Each is shown over a 60-dB range where white represents the maximum value and black represents values more than 60 dB below the maximum. Top row: Λ_A, second row: Λ_N, $\sigma_t=6$ μs; bottom row: Λ_N, $\sigma_t=3$ μs.

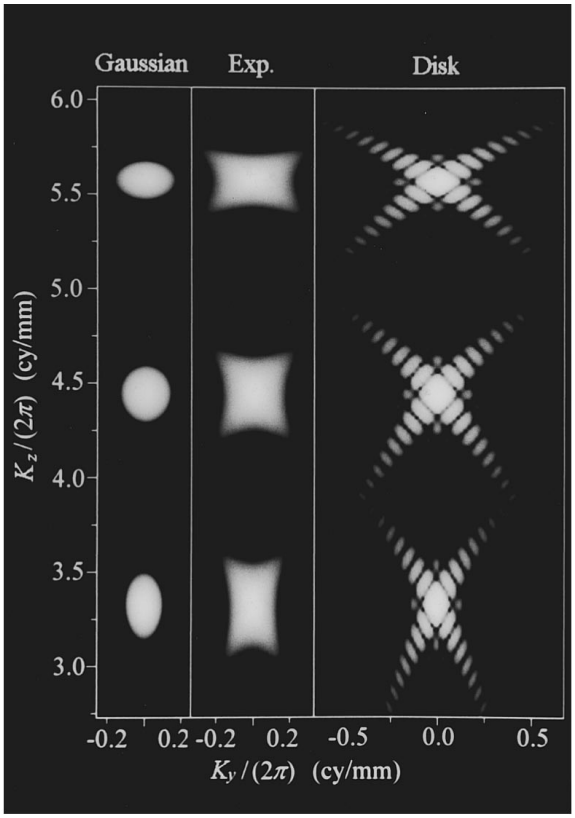

FIG. 4. System function magnitudes $|\Lambda_A|$ for 6.5-mm Gaussian, exponential, and disk apertures in angular scattering configuration. The system functions are shown in cross sections taken at the plane $K_x=0$. Each is shown over a 30-dB range where white represents the maximum value and black represents values more than 30 dB below the maximum. Each of the three panels shows $|\Lambda_A|$ for $\theta=33°$, 48°, and 60°, respectively, from top to bottom.

in practical experiments long time gates may be used in these configurations, and because the narrow-band assumption was sometimes invalidated by the considerable spread of Λ.

The system function Λ was computed by a method described previously.[18] The narrow-band system function Λ_N was obtained for the case of Gaussian time gates by implementing Eq. (11) as a convolution in the K_3 direction for each (K_1,K_2) pair.

The transfer functions H_A^V and $|H_A|^2$ were calculated for each case using the reference value $W_E(\omega_0)=1$ s. The narrow-band transfer functions H_V^N and $|H_N|^2$ were calculated for the backscatter configurations with finite time gates. The second central moments of $|\Lambda_A|^2$ and $|\Lambda_N|^2$ were computed in all three Cartesian directions for the angular scattering case, and in the axial and lateral directions for the backscatter case.

III. RESULTS

Representative system function magnitudes for the backscatter case are shown in Fig. 3. The results illustrate that increasing the length of the emitter and detector time gates decreases the spread of the system function and therefore improves wave space resolution in the K_z direction, i.e., in the direction of the reference scattering vector. Wave space resolution in the lateral direction is controlled by the aperture size and apodization; the time gate lengths have almost no effect on the resolution in this direction.

Cross-sectional renderings of the system function magnitude $|\Lambda_A|$ are shown in Fig. 4 for Gaussian, exponential, and disk apertures of radius 6.5 mm. Of particular note here is the large spread of the system function in the case of disk apertures. This large spread means that measurements nominally taken at the reference scattering vector $\mathbf{K}_0$ are blurred by spatial-frequency information far from $\mathbf{K}_0$.

Quantitative results of the computations are shown in Table I for the backscatter calculations and Table II for the angular scattering calculations. All of the reported calculations for Gaussian apertures agree with the asymptotic results [Eqs. (22)–(27)] within a fraction of 1%. The calculations for exponential and disk apertures show, for the most part, agreement with the angular dependences predicted by the asymptotic results for Gaussian apertures. The transfer functions $H_{(\cdot)}^V$ are nearly constant with angle and the transfer functions $|H_{(\cdot)}|^2$ are nearly proportional to $1/\sin(2\theta)$, as predicted by the asymptotic theory. Likewise, the total radial second central moment $\sigma=\sqrt{\sigma_1^2+\sigma_2^2+\sigma_3^2}$ is nearly constant with angle for all three apertures in the angular scattering configurations. For all the apertures in the backscatter con-

TABLE I. Radial and axial moments $\sigma_i(|\Lambda_N|^2)$ and $\sigma_i(|\Lambda_A|^2)$ and normalization factors $|H_N|^2$, $|H_A|^2$, $|H_N^V|$, and $|H_A^V|$, for identical Gaussian, exponential, and uniform apertures in backscatter configuration. The subscript A corresponds to results for infinite time gates and the subscript N corresponds to results for finite time gates obtained using the narrow-band approximation.

		Gaussian				Exponential				Uniform			
Effective radius (mm)	Time gate parameter (μs)	σ_r (cy/mm)	σ_z (cy/mm)	$\lvert H_{(\cdot)}\rvert^2$ g^2/mm μs^2	$\lvert H_{(\cdot)}^V\rvert$ g/(mm^2 μs)	σ_r (cy/mm)	σ_z (cy/mm)	$\lvert H_{(\cdot)}\rvert^2$ g^2/(mm μs^2)	$\lvert H_{(\cdot)}^V\rvert$ g/(mm^2 μs)	σ_r (cy/mm)	σ_z (cy/mm)	$\lvert H_{(\cdot)}\rvert^2$ g^2/(mm μs^2)	$\lvert H_{(\cdot)}^V\rvert$ g/(mm^2 μs)
3.175	3	0.142	0.0353	0.0213	1.75	0.149	0.0353	0.0160	1.34	0.188	0.0357	0.0206	1.91
	6	0.142	0.0177	0.171	3.50	0.149	0.0178	0.128	2.69	0.188	0.0178	0.165	3.83
	∞	0.142	0.00214	6.60	2.07	0.189	0.00707	6.60	1.59	0.187	0.0143	5.31	2.26
6.5	3	0.0693	0.0353	0.492	9.60	0.0875	0.0353	0.451	7.88	0.106	0.0354	0.361	13.0
	6	0.0693	0.0177	3.93	19.2	0.0875	0.0177	3.61	15.8	0.106	0.0179	2.89	26.0
	∞	0.0692	0.000510	110	11.3	0.0921	0.00165	113	9.31	0.0914	0.00336	92.5	15.3
10	3	0.0450	0.0353	1.50	12.4	0.0661	0.0353	1.97	15.1	0.0945	0.0354	0.766	6.84
	6	0.0450	0.0177	12.0	24.8	0.0661	0.0177	15.7	30.2	0.0944	0.0179	6.13	13.7
	∞	0.0450	0.000215	648	14.6	0.0596	0.000703	634	17.8	0.0593	0.00141	516	8.08

TABLE II. Moments $\sigma_i(|\Lambda_A|^2)$ and $\sigma(|\Lambda_A|^2)$ and normalization factors $|H_A|^2$ and $|H_A^V|$ for identical Gaussian, exponential, and uniform apertures in angular scattering configuration.

Aperture	θ (deg)	σ_x (cy/mm)	σ_y (cy/mm)	σ_z (cy/mm)	σ (cy/mm)	$\lvert H_A\rvert^2$ $g^2/(mm\ \mu s^2)$	$\lvert H_A^V\rvert$ $g/(mm^2\ \mu s)$
Gaussian	33	0.0490	0.0411	0.0267	0.0693	124	11.3
	48	0.0490	0.0328	0.0364	0.0693	114	11.3
	60	0.0490	0.0245	0.0424	0.0693	130	11.3
Exponential	33	0.0620	0.0551	0.0358	0.0903	119	9.23
	48	0.0620	0.0440	0.0488	0.0903	109	9.23
	60	0.0620	0.0328	0.0569	0.0903	126	9.23
Uniform	33	0.0665	0.0100	0.0714	0.140	95.0	15.5
	48	0.0665	0.0834	0.0892	0.139	87.2	15.5
	60	0.0665	0.0661	0.0973	0.135	100	15.5

figuration, the dependence of the moments and transfer functions on the time gate length agree closely with those predicted by the asymptotic theory.

The only notable discrepancy with the predictions of the asymptotic theory is seen in the results of the angular calculations for the disk apertures. In this case, as can be seen in Fig. 4, the spread of the system function in the K_2 and K_3 directions is considerably greater than that in the K_1 direction, while the asymptotic theory predicts that the spread is always largest in the K_1 direction. Also, for disk apertures, the total second central moment σ is larger in the angular scattering configuration than in the backscatter configuration, while the asymptotic theory predicts that it should be constant. The total second central moment is nearly constant over all angles examined for the exponential and Gaussian apertures.

The implications of these results for wave space resolution may be summarized as follows. For angular scattering measurements, the total second central moment $\sigma=\sqrt{\sigma_1^2+\sigma_2^2+\sigma_3^2}$ may be used to estimate an overall limit on the wave space resolution. Since the second central moment is approximately inversely proportional to the aperture size,[19] the 3-dB resolution limit for angular scattering measurements may be estimated (in cy/mm) as

$$\frac{\Delta K}{2\pi}=\begin{cases}2.86\sigma, & \\ 2.6r_{\mathrm{eq}}^{-1} & \text{(disk)},\\ 1.7r_{\mathrm{eq}}^{-1} & \text{(exponential)},\\ 1.3r_{\mathrm{eq}}^{-1} & \text{(Gaussian)}.\end{cases} \tag{29}$$

For backscatter measurements, σ_r is close to σ for equivalent transducers in an angular scattering configuration, so that wave space resolution in the lateral direction may be estimated using Eq. (29). More precise estimates based on the detailed calculations reported here are shown in Fig. 5.

Resolution in the direction of the scattering vector depends mainly on the characteristics of the emitted pulse and the detector gate. For a backscatter configuration employing Gaussian time gates, the 3-dB resolution limit in the axial direction is approximately

$$\Delta K/2\pi=2.86(2\pi c\alpha_t)^{-1}. \tag{30}$$

The approximate expression given in Eq. (30) agrees very well with the calculated values reported in Table I for all the apertures and time gates examined.

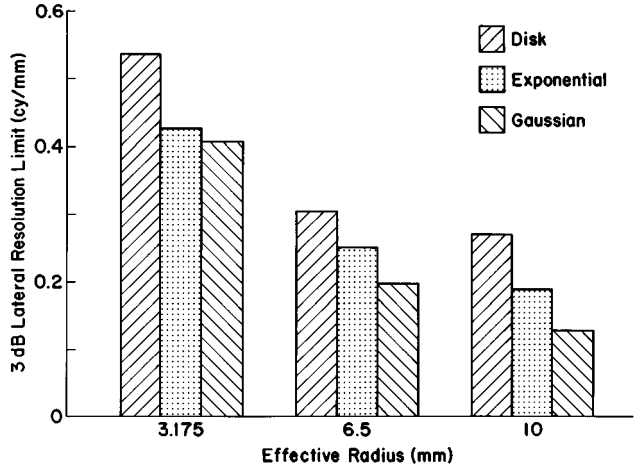

FIG. 5. Calculated lateral 3-dB resolution limit for Gaussian, exponential, and disk apertures in backscatter configuration.

IV. DISCUSSION

The results of this study may be used for quantitative estimation of the wave space resolution achievable with a given measurement system. Below, the principles of characterizing an experimental scattering configuration are illustrated by two examples.

The results of Waag *et al.*[30] provide an example of a tissue characterization experiment employing angular scattering measurements. In their study, measurements of angular scattering from calf liver were used. The emitter and detector were disk transducers of radius 3.175 mm, and the scattering volume was illuminated by tone bursts. The 3-dB resolution limit for this measurement system may be estimated from Eq. (29) as $\Delta K/(2\pi)=2.6r_0^{-1}=0.8$ cy/mm. The scanned range of spatial frequency $K/(2\pi)$ was 3.5–7.0 cy/mm. Thus the measured spatial-frequency information was blurred over scales on the order of 0.8 cy/mm, so that spatial-frequency features of smaller scale than this were not resolvable. However, since the resolution limit was consid-

erably smaller than the range scanned, the measured spectra accurately characterized spatial-frequency variations on scales larger than 0.8 cy/mm.

As an example of a tissue characterization experiment employing backscatter measurements, the study of Zagzebski *et al.*[31] may be examined. In this study, backscatter from human liver tissue was measured *in vivo* using a commercial scanner. Real-space images were also formed using the scattering data, so that wideband pulses and relatively short time gates were used in order to increase the real-space resolution. Time gating was performed with a Blackman–Harris window of length 4 μs applied in software postprocessing. Broadband backscatter signals were decomposed into frequency components over the range 2.25–3.75 MHz, which corresponds to a spatial-frequency range of 3.0–5.0 cy/mm.

The effect of the windowing may be estimated using the results reported here for Gaussian time gates. Since the emitted pulses were wideband, the combined effect of the emitter and detector time gates may be approximated by that of the detector gate alone. In this case, the wave space resolution in the axial direction can be obtained from the formulas given above for the case of identical emitter and detector time gates with α_t replaced by $\alpha_t/\sqrt{2}$.

The Blackman–Harris window used by Zagzebski *et al.* corresponds best (in the least-mean-square error sense) to a Gaussian time gate with $\alpha_t=0.680$ μs. The 3-dB resolution limit in the direction of the scattering vector is, using Eq. (30), approximately 0.63 cy/mm and the estimated absolute resolution limit is 0.44 cy/mm. The frequency step in this study was 0.25 MHz, which corresponds to a spatial-frequency increment of 0.33 cy/mm. Thus their measured backscatter data were somewhat blurred by system effects over a range on the order of one spatial-frequency step. However, as in the case of Ref. 30, the scale of the spatial-frequency blur was considerably smaller than the extent of the spatial-frequency range examined, so that the measured frequency-dependent backscatter coefficient can still be interpreted as an accurate estimation of the tissue spatial-frequency spectrum. The resolution limit calculated here is consistent with Zagzebski's empirical observation that window lengths smaller than 4 μs resulted in inadequate determination of the frequency dependence of backscatter for a frequency step of 0.5 MHz (corresponding to a spatial-frequency step of 0.67 cy/mm).[31]

In the present study, attenuation of scattering objects was not considered. Although attenuation would affect the magnitudes of the transfer functions derived here, the present results for wave space resolution are still valid for weakly attenuating media. More specifically, the wave space resolution effects described here are not significantly changed by attenuation as long as the length scale over which the attenuation occurs is considerably larger than the correlation length of the scattering medium variations. Since tissue is weakly attenuating over the range of ultrasonic frequencies relevant for tissue characterization, the wave space resolution results presented here are expected to be valid for ultrasonic scattering by tissue.

Although the theory presented here provides extensive insight about the spatial-frequency blur caused by measurement system effects, the full computations reported here are not an ideal approach to normalization of scattering measurements. Calculation of the exact normalization factors $|H_{(\cdot)}|^2$ and $H^V_{(\cdot)}$ requires extensive computations. For example, the computations reported here typically required 1–12 h of CPU time on an IBM ES 9000 computer.

For this reason, calculation of normalization factors using the full integral expressions is most useful as a benchmark for simplified, more computationally efficient methods. When the accuracy of approximations made is verified using such a benchmark, reasonable accuracy may be obtained conveniently from the asymptotic formulas given here for Gaussian apertures and time gates [Eqs. (22)–(25)], since the results for all apertures had nearly the angle and time gate dependence predicted by the asymptotic Gaussian theory. The differences in magnitude of the normalization integrals may be removed by any calibration procedure that uses a known scattering object, e.g., a perfect reflector.

The results of the present study have important implications for tissue characterization measurements. The calculations show that accurate determination of the spectral features of tissue properties requires a tight concentration of the emitter and detector beam patterns in wave space, which in turn requires a broad region of plane-wave-like illumination in real space. Because of this trade-off between real-space and wave space resolution, high spatial resolution ultrasonic measurements such as those used in conventional b-scan imaging are not well suited for tissue characterization techniques of the type discussed here. This trade-off also limits the quality of any quantitative imaging system in which real-space images of scattering object properties are made using the principles of tissue characterization as discussed in the present paper.

A further implication for tissue characterization is that small regions of tissue cannot easily be characterized using the methods discussed here. For instance, a tumor in the early stages of growth may not be sufficiently large to comprise a scattering region of the size needed for good wave space resolution. Tissue characterization techniques such as those reported here do, however, have potential for diagnosis of diffuse disease in relatively isotropic tissue such as liver.

V. CONCLUSION

Spatial-frequency resolution of scattering measurement systems for tissue characterization has been analyzed using wave space representations of emitter and detector beam patterns and time gates. The theory explicitly characterizes the wave space resolution achievable with a given scattering measurement system in either backscatter or angular scattering configurations.

Detailed computations of measurement system effects have been performed for Gaussian, exponential, and disk apertures for three transducer sizes in a backscatter configuration and for three angles in an angular scattering configuration. The computations show the nonuniform weight imposed by measurement system effects on estimates of spatial-frequency scattering medium properties. In the case of disk apertures, this weight extends over a region of wave

space that is large compared to the region where the weight is mainly concentrated.

The computational and theoretical results show that wave space resolution increases with aperture size and that smooth transducer apodization also increases resolution. In the case of backscatter measurements, axial resolution is determined by the time gate lengths while lateral resolution is determined by the apertures. In all cases, system requirements for high spatial-frequency resolution are converse to those required for high spatial (imaging) resolution. In other words, high spatial-frequency resolution requires broad, plane-wave-like beams and long time gates, while high spatial resolution requires tightly focused beams and short time gates.

ACKNOWLEDGMENTS

The authors thank Andrew K. Halberstadt, who provided help during the initial stages of the research reported here. Helpful discussions with Jeffrey P. Astheimer are acknowledged with pleasure. Consultations with Dong-Lai Liu, Richard A. Phillips, and Timothy J. Case are gratefully acknowledged. Funding for this work was provided by the F. V. Hunt Fellowship of the Acoustical Society of America, the University of Rochester Diagnostic Ultrasound Research Laboratory Industrial Associates, NIH Grants No. DK 45533 and No. HL 150855, and US Army Grant No. DAMD 17-94-J-4384. Computations were performed at the Cornell National Supercomputing Facility, which is supported in part by the National Science Foundation, New York State, and the IBM corporation.

[1] B. D. Cullity, *Elements of X-Ray Diffraction* (Addison-Wesley, Reading, MA, 1978), 2nd ed.

[2] R. C. Chivers, R. R. Hill, and D. Nichols, ''Frequency dependence of ultrasonic backscattering cross-section: an indicator of tissue structure characteristics,'' *Proceedings of the Second World Congress on Ultrasonics in Medicine* (Excerpta Medica, Amsterdam, 1973), pp. 300–303.

[3] R. C. Waag and R. M. Lerner, ''Tissue macrostructure determination with swept-frequency ultrasound,'' *IEEE Ultrasonics Symposium Proceedings* (IEEE, New York, 1973), IEEE Cat. No. 73 CHO 807-8SU, pp. 63–66.

[4] R. C. Chivers and C. R. Hill, ''A spectral approach to ultrasonic scattering from human tissue: methods, objectives, and backscattering measurements,'' Phys. Med. Biol. **20**, 799–815 (1975).

[5] D. Nichols, ''Orientation and frequency dependence of backscattered energy and its clinical application,'' in *Recent Advances in Ultrasound in Biomedicine*, edited by D. N. White (Research Studies, Forest Grove, OR, 1977), pp. 29–54.

[6] R. C. Waag, R. M. Lerner, P. P. K. Lee, and R. Gramiak, ''Ultrasonic Diffraction Characterization of Tissue,'' in *Recent Advances in Ultrasound in Biomedicine*, edited by D. N. White (Research Studies, Forest Grove, OR, 1977), Vol. 1, pp. 87–116.

[7] R. A. Sigelmann and J. M. Reid, ''Analysis and measurement of ultrasound backscattering from an ensemble of scatterers excited by sine-wave bursts,'' J. Acoust. Soc. Am. **53**, 1351–1355 (1973).

[8] M. O'Donnell and J. G. Miller, ''Quantitative broadband ultrasonic backscatter: an approach to nondestructive evaluation in acoustically inhomogeneous materials,'' J. Appl. Phys. **52**, 1056–1065 (1981).

[9] D. Nichols and C. R. Hill, ''Evaluation of backscattering coefficients for excised human tissues: principles and techniques,'' Ultrasound Med. Biol. **8**, 7–15 (1982).

[10] F. L. Lizzi, M. Greenebaum, E. J. Feleppa, and M. Elbaum, ''Theoretical framework for spectrum analysis in ultrasonic tissue characterization,'' J. Acoust. Soc. Am. **73**, 1366–1373 (1983).

[11] M. A. Fink and J. F. Cardoso, ''Diffraction effects in pulse-echo measurements,'' IEEE Trans. Son. Ultrason. **SU-31**, 313–329 (1984).

[12] E. L. Madsen, M. F. Insana, and J. A Zagzebski, ''Method of data reduction for accurate determination of acoustic backscatter coefficients,'' J. Acoust. Soc. Am. **75**, 913–923 (1984).

[13] M. F. Insana, R. F. Wagner, D. G. Brown, and T. J. Hall, ''Describing small-scale structure in random media using pulse-echo ultrasound,'' J. Acoust. Soc. Am. **87**, 179–192 (1990).

[14] M. F. Insana, T. J. Hall, and L. T. Cook, ''Backscatter coefficient estimation using array transducers,'' IEEE Trans. Ultrason. Ferroelecr. Frequency Control **41**, 714–723 (1994).

[15] J. Meunier and M. Bertrand, ''Echographic image mean gray level changes with tissue dynamics: a system-based model study,'' IEEE Trans. Biomed. Eng. **42**, 403–410 (1995).

[16] J. A. Campbell and R. C. Waag, ''Normalization of ultrasonic scattering measurements to obtain average differential scattering cross sections for tissues,'' J. Acoust. Soc. Am. **74**, 393–399 (1983).

[17] P. K. Nassiri and C. R. Hill, ''The differential and total bulk acoustic scattering cross sections of some human and animal tissues,'' J. Acoust. Soc. Am. **79**, 2034–2047 (1986).

[18] R. C. Waag and J. P. Astheimer, ''Characterization of measurement system effects in ultrasonic scattering experiments,'' J. Acoust. Soc. Am. **88**, 2418–2436 (1990).

[19] R. C. Waag, J. P. Astheimer, and J. F. Smith III, ''Analysis and computations of measurement system effects in ultrasonic scattering experiments,'' J. Acoust. Soc. Am. **91**, 1284–1297 (1992).

[20] K. Chandra and C. Thompson, ''Ultrasonic characterization of fractal media,'' Proc. IEEE **81**, 1523–1533 (1993).

[21] R. Gramiak, R. C. Waag, E. A. Schenk, P. P. K. Lee, K. Thomson, and P. Macintosh, ''Ultrasonic detection of myocardial infarction by amplitude analysis,'' Radiology **130**, 713–720 (1979).

[22] D. Y. Fei, K. K. Shung, and T. M. Wilson, ''Ultrasonic backscatter from bovine tissues: Variation with pathology,'' J. Acoust. Soc. Am. **81**, 166–172 (1987).

[23] K. A. Wear, M. R. Milunski, S. A. Wickline, J. E. Perez, B. E. Sobel, and J. G. Miller, ''Differentiation between acutely ischemic myocardium and zones of completed infarction in dogs on the basis of frequency-dependent backscatter,'' J. Acoust. Soc. Am. **85**, 2634–2641 (1989).

[24] J. C. Bamber and C. R. Hill, ''Acoustic properties of normal and cancerous human liver—I. Dependence of pathological conditions,'' Ultrasound Med. Biol. **7**, 121–133 (1981).

[25] R. Momenan, R. F. Wagner, B. S. Garra, M. H. Loew, and M. F. Insana, ''Image staining and differential diagnosis of ultrasound scans based on the Mahalanobis distance,'' IEEE Trans. Med. Imag. **13**, 37–47 (1994).

[26] D. Zatari, N. Botros, and F. Dunn, ''*In vivo* liver differentiation by ultrasound using an artificial neural network,'' J. Acoust. Soc. Am. **96**, 376–381 (1994).

[27] T. M. Burke, T. A. Blankenberg, A. K. Q. Siu, F. G. Blankenberg, and H. M. Jensen, ''Preliminary investigation of ultrasound scattering analysis to identity women at risk for later invasive cancer. II: Extraction of dominant scattering angle-dependent trends from excised breast tissue,'' Ultrasound Med. Biol. **21**, 305–311 (1995).

[28] B. Hete and K. K. Shung, ''A study of the relationship between mechanical and ultrasonic properties of dystrophic and normal skeletal muscle,'' Ultrasound Med. Biol. **21**, 343–352 (1995).

[29] P. M. Morse and K. U. Ingard, *Theoretical Acoustics* (McGraw-Hill, New York, 1968), pp. 407–418.

[30] R. C. Waag, D. Dalecki, and P. E. Christopher, ''Spectral power determinations of compressibility and density variations in model media and calf liver using ultrasound,'' J. Acoust. Soc. Am. **85**, 423–431 (1989).

[31] L. A. Zagzebski, Z. F. Lu, and L. X. Xao, ''Quantitative ultrasound imaging: *in vivo* results in normal liver,'' Ultrason. Imag. **15**, 335–351 (1993).